Defect level identification of ATLAS ITk Strip Sensors using DLTS

C.T. Klein[a,*], J. Dandoy[a], D. Duvnjak[a], V. Fadeyev[b], K. Hara[c], S. Hirose[c], C. Jessiman[a], J.S. Keller[a], T. Koffas[a], K. Nakamura[d], E. Staats[a], M. Ullan[e], Y. Unno[d], R. Vandusen[a]

[a] *Herzberg Laboratory, Carleton University, 1125 Colonel By Dr., Ottawa, ON, K1S 5B6, Canada*
[b] *Santa Cruz Institute for Particle Physics (SCIPP), University of California, Santa Cruz, CA 95064, USA*
[c] *Institute of Pure and Applied Sciences, University of Tsukuba, 1-1-1 Tennodai, Tsukuba, Ibaraki 305-8571, Japan*
[d] *Institute of Particle and Nuclear Study, KEK, 1-1 Oho, Tsukuba, Ibaraki 305-0801, Japan*
[e] *Instituto de Microelectronica de Barcelona (IMB-CNM, CSIC), Campus UAB-Bellaterra, 08193 Barcelona, Spain*

Abstract

As a part of ongoing studies in parallel to ITk Strip Sensor Production quality control (QC) and quality assurance (QA), diodes fabricated as test structures were measured using *Deep-Level Transient Spectroscopy* (DLTS). This was done to achieve precise sensor simulations motivated by findings of anomalous leakage current behaviour, as well as to compile a more complete model of radiation damage in ITk Strip Sensors. Utilising DLTS spectra with varying test parameters, trap energy levels and cross-sections associated with defects in the devices were obtained. Furthermore, employing related measurements techniques, such as Thermal Admittance Spectroscopy (TAS), results were supplemented and expanded, or additional points of interest, such as the deep level profile and the capture kinematics of the trap levels, were investigated with double-pulse DLTS (DDLTS). A common trap consistent with a C_iO_i point defect in unirradiated diodes was identified, but also an additional trap suspected to cause high leakage current. In proton-irradiated diodes, defects related to vacancy clusters or a boron-hydrogen complex were observed.

Keywords: HL-LHC, ATLAS, ITk, DLTS

ATL-ITK-PROC-2024-005
12 February 2024

1. Introduction

The current ATLAS Inner Detector [1] will have reached the end of its lifespan and will be rendered inoperable with the increased luminosity, associated data rate, and radiation damage in the HL-LHC upgrade. Therefore the Inner Detector will be replaced with the new all-silicon ATLAS Inner Tracker (ITk) [2], consisting of the inner Pixel Detector and the outer Strip Detector. The Strip Detector is further divided into the cylindrical barrel region around the interaction point, consisting of four layers of staves made of 14 modules per face of the stave, and six disks in the forward end-cap region arranged from petals with nine endcap modules on each face, with a total silicon area of 165 m^2. ITk strip sensors are single-sided n^+-in-p sensors with square shape in the barrel region and wedge shape with curved edges at constant radius in the end-cap. The properties of all sensor layouts and the assembled detector are detailed in [3].

*Corresponding author
Email address: christoph.klein@cern.ch (C.T. Klein)

During the currently ongoing sensor production phase, full-size main sensors were tested for mechanical and electrical compliance with technical specifications, the quality control (QC), while fabrication parameters and post-irradiation performance were verified on test structures from the same wafers, the quality assurance (QA). Part of those test structures are square diodes of different dimensions, some of which were measured using *Deep-Level Transient Spectroscopy* (DLTS) [4]. This was done to achieve precise sensor simulations motivated by findings of anomalous leakage current behaviour, as well as to compile a more complete model of radiation damage in ITk Strip Sensors.

The diode samples used for DLTS measurements are produced on the same wafers as the full-size strip sensors and located on the wafer *halfmoons* that were surrounding the main sensor[5]. For DLTS measurements the 8 mm × 8 mm *MD8 diodes* are cleaved out from either the unirradiated halfmoons or after irradiation from the QA test piece shown in Fig. 1(a). Unirradiated diodes mostly stemmed from a batch containing a significant number of main sensors with anomalously high leakage current about a factor of 2 higher than

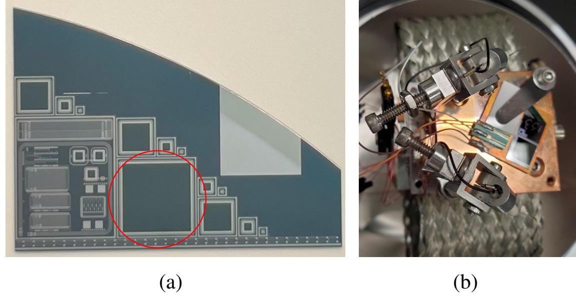

(a) (b)

Figure 1: (a): QA test piece with a *test chip* structure and diodes of different dimensions. The MD8 diode used for DLTS measurements is highlighted with a red circle. (b): Temperature-controlled DLTS stage inside the cryostat with a mounted diode sample.

typical, but still well within specifications. For comparison, reference samples from a batch with average results during QC were also included. Irradiation for the irradiated samples was performed with the 70 MeV proton beam provided by the Cyclotron and Radioisotope Center (CYRIC) of Tohoku University (Japan) as part of the regular QA procedure to three different fluences of 4.57×10^{14} n_{eq}/cm^2, 8.34×10^{14} n_{eq}/cm^2, and 1.54×10^{15} n_{eq}/cm^2 (10% uncertainty). After irradiation, all samples were annealed for 80 min at 60 °C. The cleaved-out MD8 diodes are glued to a heatsink, and cathode and GR contacts wire-bonded to a small piece of PCB providing cable connections before being placed on the stage inside the DLTS cryostat (see Fig. 1(b)).

2. IV and CV measurement

Before conducting the actual DLTS measurements, the leakage current and capacitance of all samples is measured as a function of the applied bias voltage (IV and CV, respectively). In the case of diode samples investigated after irradiation, this has also been done by default as part of the QA testing procedure.

Fig. 2(a) shows the IV curves of all unirradiated diode samples taken in the DLTS setup at room temperature. Samples with wafer numbers W153, W154, W156 stemmed from the same wafers as main sensors observed to exhibit anomalously high leakage current, while W178 and W179 were also from the same batch, albeit having typical leakage current levels. Wafers W418 to W421 originated from a different batch as reference, so as to compare the DLTS results and correlate the occurrence of high leakage current with the presence of specific defects. As can be seen in Fig. 2(a), only W153 of the anomalous batch had a much higher leakage current while W418 and W420 showed similarly

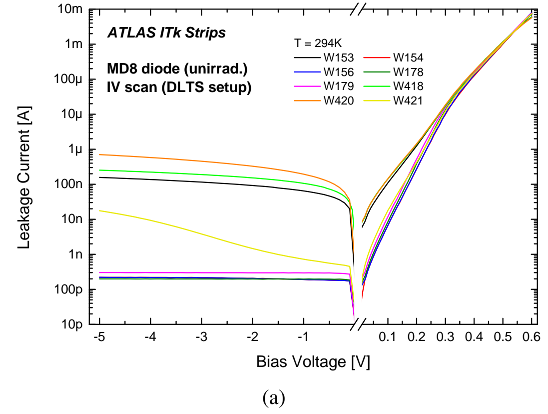

(a)

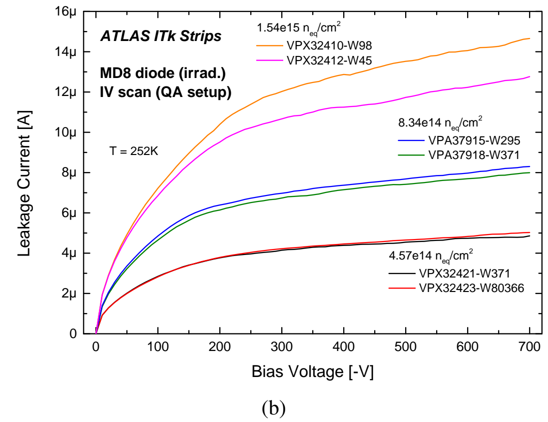

(b)

Figure 2: (a): IV characteristic of unirradiated diode samples taken in the DLTS setup at room temperature. (b): IV measurements taken for all irradiated samples as part of sensor QA.

high current, unlike their full-size counterparts. The IV results for irradiated diodes displayed in Fig. 2(b) were taken during QA measurements and display the clear scaling of the leakage current with fluence.

CV results did not show any significant difference between unirradiated diodes. Two examples are shown in Fig. 3(a), taken in the DLTS setup at room temperature, for which the depletion width and carrier concentration have been derived from the measured capacitance values. The CV characteristics of the irradiated samples taken during QA shown in Fig. 3(b) do not appear to depend on fluence levels of the samples. Full depletion is still achieved even at the highest irradiation level available and values of both full depletion voltage and effective doping concentration are similar to unirradiated samples of the same sensor batches. This indicates that there has only been a very limited defect introduction from the irradiation process.

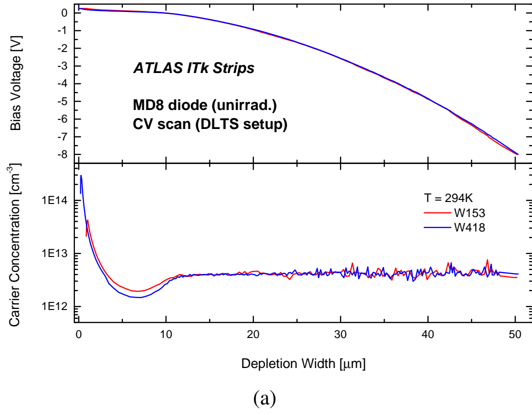

(a)

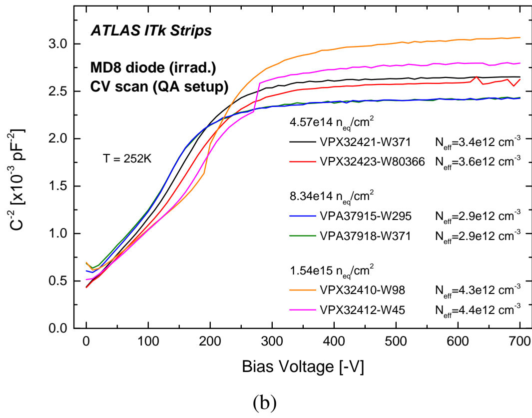

(b)

Figure 3: (a): CV results of two unirradiated diode samples at 50 kHz converted into the dependence of applied bias voltage and the depletion width achieved, and the profile of carrier concentration as a function of the depletion width. (b): CV measurements taken for all irradiated samples as part of sensor QA at 2 kHz, plotted as C^{-2} vs. V.

3. DLTS results of unirradiated diodes

The experimental setup for measuring DLTS spectra at Carleton University allowed for reliable operation in cryogenic temperatures as low as approximately 35K with the given samples. Measurements above room temperature were only done in a limited range to prevent excessive leakage current. Bias voltage during scans, both for unirradiated and irradiated diodes, was optimised to achieve saturation of the transient amplitude. Typically, a few hundred transients were recorded for each temperature point and the resulting average used for analysis to reduce measurement noise. DLTS spectra were analysed using the double-boxcar method described in [4], by varying the rate window corresponding to the emission rate of traps in the material. For unirradiated diodes, standard Capacitance-DLTS (C-DLTS or just DLTS) yielded the best results.

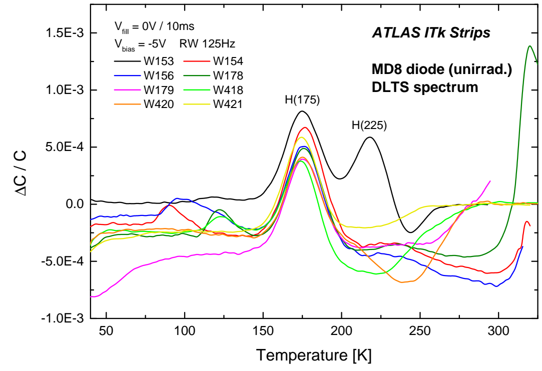

Figure 4: DLTS spectra of unirradiated diodes.

The DLTS spectra of all unirradiated diodes for a select rate window are shown in Fig. 4. All diodes have been tested at different bias voltage and filling pulse settings, but there was no qualitative change in results, only a saturation of peak heights for increasing reverse bias. The negative offset seen in the spectra was mitigated by grounding the diode guard ring, but this also did not affect the overall results of the subsequent Arrhenius analyses and corresponding trap parameters. As all samples are n^{+}-in-p diodes, the peaks seen in the spectra each represent one hole (majority carrier) trap in the p-type bulk material. In the case of peaks being a convolution of multiple trap states with peak temperatures in close proximity, they could be separated through Gaussian deconvolution in the peak analysis process.

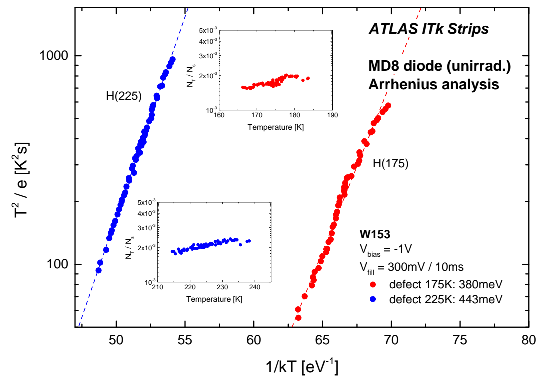

Figure 5: Arrhenius plots for the defects observed in the DLTS spectrum of unirradiated diode W153. The small inset graphs show the relative trap concentration for each data point.

All samples shared a common peak H(175) which contained one trap state. Smaller peaks seen for some samples at low temperatures around 100 K in Fig. 4 were either artefacts of the displayed rate window or vanished with slight variations of measurement param-

eters, and could therefore not be used to derive a clear Arrhenius plot. The only other additional defect seen in unirradiated samples was H(225) exclusively observed in W153 and confirmed over multiple runs using two different diode samples. Arrhenius plots for both defects of W153 are shown in Fig. 5 and trap parameters are summarised in Tab. 1. The small inset graphs in Fig. 5 show the relative trap concentrations and their flat temperature dependence serve as an indicator that the trap states had achieved a good saturation under the measurement parameters used.

Aside from standard DLTS measurements, *Double-Pulse DLTS* (DDLTS) measurements at the temperature of traps observed in the spectrum were performed to obtain further information of the underlying trap states. For the unirradiated diode samples, the *deep level trap profile* [6] and the *capture kinematics* [7] were investigated. The former was done by using a progressively increasing filling pulse at fixed bias and evaluating the signal difference between adjacent filling pulse voltages as a function of the depletion width extracted from CV measurements (see Fig. 3(a)). The latter was determined by using an increasing filling pulse duration over multiple orders of magnitude, where the transient amplitude saturation rate can indicate whether in the crystal lattice the corresponding trap is caused e.g. by point defects, dislocations, or discrete energy barriers.

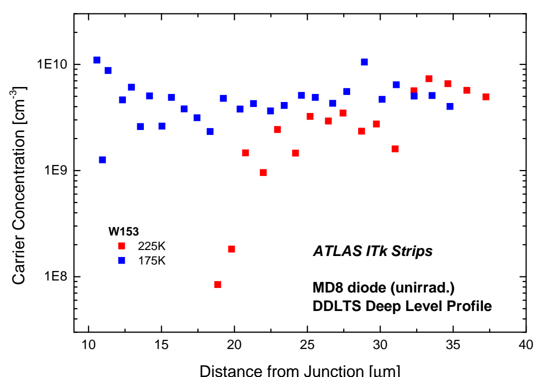

Figure 6: Deep level profile of the two traps observed in diode W153.

The deep level profile, shown in Fig. 6 for diode W153 as an example, of the common trap H(175) appeared to be constant throughout the measured range of bulk depth. In contrast to this, the trap concentration of H(225), the sole other trap state unique to W153, decreased significantly close to the junction of the diode. When comparing the saturation rate for all measured traps to simulated data of the capture process for different defect types, the observed very fast saturation for filling pulses $t_{fill} \gtrsim 1$ ms, as seen for H(225) in Fig. 7, indicated a point defect as the underlying cause for both the common H(175) as well as H(225).

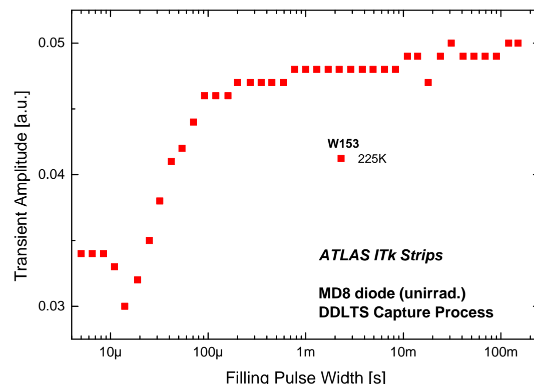

Figure 7: Transient amplitude saturation defect H(225) as a function of the filling pulse width.

4. DLTS results of irradiated diodes

Due to high trap concentration and large increase in leakage current, which lead to insufficient trap saturation in standard DLTS measurements, *Current DLTS* (I-DLTS) was instead used to obtain trap parameters in the proton-irradiated diode samples.

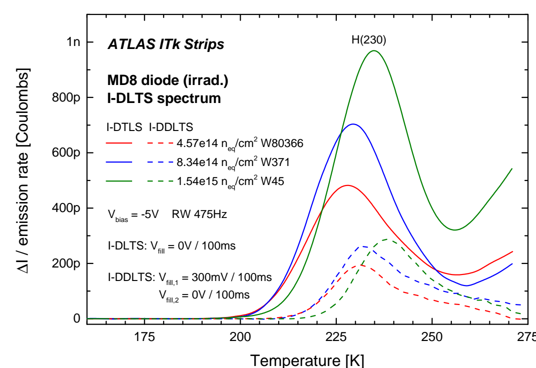

Figure 8: I-DTLS (solid lines) and I-DDLTS (dashed lines) spectra of irradiated diodes.

Fig. 8 shows the I-DLTS spectra of three irradiated diodes, one of each fluence available, as the plots with solid lines. As can be seen, the spectrum shows a very clear single peak denoted H(230) with a subsequent rise at higher temperatures that could not be explored further due to the exponentially increasing leakage current at those temperatures. The resulting Arrhenius plots can be seen in Fig. 9(a) and the trap parameters are summarised in Tab. 1.

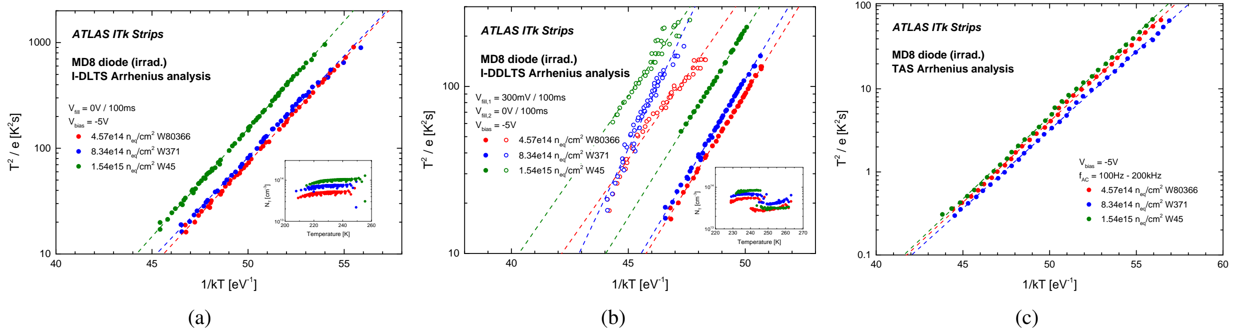

Figure 9: Arrhenius plots derived from the spectra of irradiated diodes obtained from I-DLTS (a), I-DDLTS (b), and TAS (c) measurements. In (b): closed circles are from the peak, open circles from the secondary component in the slowly falling flank.

In addition, other modes of data taking were explored, one of which uses a double filling pulse to eliminate the leakage current baseline, potentially resulting in a clearer spectrum or one with additional observable traps. For the available irradiated diodes, this mode was successfully used in conjunction with a forward bias injection pulse to uncover a slowly falling flank in the I-DDLTS spectrum, indicating additional traps contributing at that temperature range. The I-DDLTS spectra are displayed as dashed lines in Fig. 8 and using a 2-Gaussian deconvolution, the corresponding Arrhenius plots of the two trap states derived from the spectra are shown in Fig. 9(b). Due to the more complicated analysis method, the resulting trap parameters of the slow falling flank, listed in Tab. 1, have significantly larger uncertainties, therefore future investigations will focus on improving measurements of the secondary peak components.

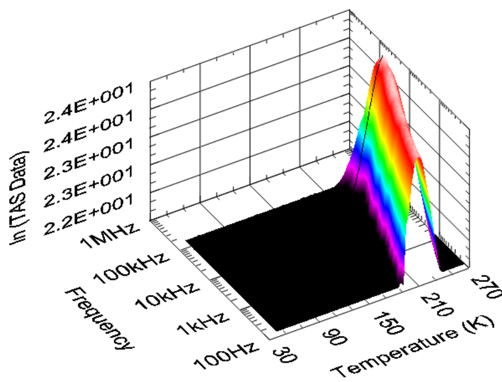

Figure 10: TAS results of an irradiated diode showing the dependence of the peak as a function of temperature and test signal frequency.

Lastly, the proton-irradiated diodes samples were measured using *Thermal Admittance Spectroscopy* (TAS) [8]. This measurement is different from the other employed spectroscopy methods, as it does not rely on a single measured quantity like current, but rather measures capacitance, resistance, conductivity, and phase together as a function of both temperature and AC test signal frequency. Furthermore, it is a steady-state measurement that does not record fast transients and instead determines the thresholds of defect contributions through steps or peaks in the temperature dependence of the TAS signal. With this different approach, TAS can be used to either verify DLTS results or complement those findings, and it is particularly useful for high-resistivity materials like the ones used for ITk sensors. An example for the TAS signal of the resistance of an irradiated diode is shown in Fig. 10, while the Arrhenius plots can be seen in Fig. 9(c), and the trap parameters in Tab. 1.

5. Discussion and summary

Multiple defect states have been identified during the detailed measurements of both unirradiated and proton-irradiated MD8 diodes produced on the same wafers as main ATLAS ITk Strip Sensors. The trap parameters have been determined using a variety of spectroscopy methods and all findings are summarised in Tab. 1.

In all unirradiated diodes a common point defect H(175) was observed. The trap parameters of this state are consistent with results reported in the past for the interstitial carbon - interstitial oxygen (C_iO_i) or vacancy-carbon-oxygen complex [9, 10]. The common H(230) seen in I-DLTS and TAS measurements of proton-irradiated diodes, but also point defect H(225) unique to the unirradiated W153 sample, has a trap energy and peak temperature similar to defects associated with vacancy clusters [11]. Moreover, similar defects were found to be responsible for current generation in

Table 1: Summary of all trap parameters obtained.

$\Phi[n_{eq}/cm^2]$	Meas. setup	T_{peak} [K]	E_{Trap} [meV]	$\ln\left(\sigma[cm^2]\right)$
unirradiated	DLTS	175 (common)	E_V + (310 to 390)	−32.2 to −29.9
	DLTS	225 (W153 only)	$E_V + 443 \pm 6$	-32.5 ± 0.3
4.57×10^{14}	I-DLTS	229	$E_V + 452 \pm 4$	-31.2 ± 0.2
	I-DDLTS	234	$E_V + 521 \pm 7$	-28.0 ± 0.3
	I-DDLTS	248	$E_V + 457 \pm 28$	-32.6 ± 1.3
	TAS	230	$E_V + 449 \pm 6$	-28.5 ± 0.3
8.34×10^{14}	I-DLTS	228	$E_V + 442 \pm 7$	-31.8 ± 0.4
	I-DDLTS	237	$E_V + 539 \pm 9$	-27.3 ± 0.4
	I-DDLTS	254	$E_V + 686 \pm 42$	-22.4 ± 1.9
	TAS	228	$E_V + 435 \pm 4$	-28.9 ± 0.2
1.54×10^{15}	I-DLTS	233	$E_V + 469 \pm 3$	-31.1 ± 0.2
	I-DDLTS	238	$E_V + 516 \pm 6$	-29.1 ± 0.3
	I-DDLTS	251	$E_V + 465 \pm 41$	-33.1 ± 1.9
	TAS	232	$E_V + 456 \pm 5$	-28.2 ± 0.3

CMS test structures with high leakage current [12]. It can be concluded that for wafer W153 this bulk trap is the cause for high leakage current, while in the other high-current samples likely causes are e.g. surface defects. Lastly, a defect similar to the primary trap in the I-DDLTS results has been previously observed with it being related to a boron and hydrogen complex [13].

Acknowledgements

This work was supported by the Canada Foundation for Innovation and the Natural Sciences and Engineering Research Council of Canada; the Spanish R&D grant PID2021-126327OB-C22, funded by MCIN/AEI/10.13039/501100011033 / FEDER, UE; the US Department of Energy, grant DE-SC0010107; the Grant-in-Aid for scientific research on advanced basic research (Grant No. 19H05193, 19H04393, 21H0073 and 21H01099) from the Ministry of Education, Culture, Sports, Science and Technology, of Japan. In keeping the research program move forward, the Cyclotron Radio Isotope Center (CYRIC) at Tohoku University was very important to this project.

Copyright 2024 CERN for the benefit of the ATLAS Collaboration. Reproduction of this article or parts of it is allowed as specified in the CC-BY-4.0 license.

References

[1] ATLAS Collaboration, The ATLAS experiment at the CERN large hadron collider, J. Inst. 3 (08) (2008) S08003–S08003.

[2] ATLAS Collaboration, Technical Design Report for the ATLAS Inner Tracker Strip Detector, Tech. Rep. CERN-LHCC-2017-005. ATLAS-TDR-025, CERN, Geneva (2017).

[3] Y. Unno, et al., Specifications and pre-production of n^+-in-p large-format strip sensors fabricated in 6-inch silicon wafers, atlas18, for the inner tracker of the atlas detector for high-luminosity large hadron collider, J. Inst. 18 (03) (2023) T03008.

[4] D. V. Lang, Deep-level transient spectroscopy: A new method to characterize traps in semiconductors, J. Appl. Phys. 45 (7) (1974) 3023–3032.

[5] S. Hirose, et al., ATLAS ITk strip sensor quality assurance tests and results of ATLAS18 pre-production sensors, JPS Conf. Proc.VERTEX2022 proceedings, submitted for printing (2023).

[6] Y. Zohta, M. O. Watanabe, On the determination of the spatial distribution of deep centers in semiconducting thin films from capacitance transient spectroscopy, J. Appl. Phys. 53 (3) (1982) 1809–1811.

[7] D. Pons, Accurate determination of the free carrier capture kinetics of deep traps by space-charge methods, J. Appl. Phys. 55 (10) (1984) 3644–3657.

[8] D. L. Losee, Admittance spectroscopy of impurity levels in Schottky barriers, J. Appl. Phys. 46 (5) (1975) 2204–2214.

[9] P. M. Mooney, et al., Defect energy levels in boron-doped silicon irradiated with 1-mev electrons, Phys. Rev. B 15 (1977) 3836–3843.

[10] H. T. Danga, et al., Electrically active defects in p-type silicon after alpha-particle irradiation, Physica B: Condensed Matter 535 (2017) 99–101.

[11] A. Himmerlich, et al., Defect characterization studies on irradiated boron-doped silicon pad diodes and low gain avalanche detectors, Nucl. Instrum. Methods Phys. Res. A 1048 (2023) 167977.

[12] A. Junkes, Influence of radiation induced defect clusters on silicon particle detectors, Ph.D. thesis, Universität Hamburg, Hamburg (2011).

[13] F. Volpi, A. R. Peaker, I. Berbezier, A. Ronda, Electrically active defects induced by sputtering deposition on silicon: The role of hydrogen, J. Appl. Phys. 95 (9) (2004) 4752–4760.